Structure and dynamics of a nanocolloidal silica gel dispersion

A. Roshi, S. Barjami, and G. S. Iannacchione*
Department of Physics, Worcester Polytechnic Institute, Worcester, Massachusetts 01609, USA

D. Paterson and I. McNulty
Experimental Facilities Division, Argonne National Laboratory, Argonne, Illinois 60439, USA
(Received 9 February 2006; revised manuscript received 20 July 2006; published 21 September 2006)

We studied the structure and the dynamics of a nanocolloidal silica gel dispersed in an organic solvent [octylcyanobiphenyl (8CB)] as a function of the silica density by x-ray intensity fluctuation spectroscopy (XIFS). The silica density of the dispersed aerosil gel samples ranged from 0.03 to 0.20 g cm^{-3} and the autocorrelation of the silica scattering was probed over the q range from 0.03 to 0.15 nm^{-1} (corresponding to length scales from 42 to 209 nm) at a constant room temperature at which 8CB is in the smectic-*A* phase. The gel structure has a fractal dimension in this density range of $d_f \simeq 2.15$. The time autocorrelation functions of the gels show clear density-dependent and complex dynamics. The gel relaxation times are very long and become bimodal with nonergodic character for densities from 0.10 to 0.16 g cm^{-3}. In this same density range, the fluctuation contrast (strength) is a minimum while the relaxation time becomes independent of wave vector. Together, these results indicate that there is a narrow silica density range for these gels in which the dynamics changes dramatically. This suggests a complex phase diagram for the dynamics of aerosil gels as a function of densification.

DOI: 10.1103/PhysRevE.74.031404 PACS number(s): 61.10.−i, 61.43.Hv, 67.40.Fd, 82.70.Gg

I. INTRODUCTION

In recent years, the structure and dynamics of colloidal gels have received a great deal of attention. This is due to such systems standing at the crossroads of materials science, polymer physics, and biophysics. Better understanding of such systems is likely to have a dramatic impact on the paint, adhesive, cosmetics, and dental hygiene industries, to name a few. Of particular interest are colloidal gels formed from hydrogen-bonded silica aerosils leading to fractal structures by some limited aggregation processes [1]. Such gels have a thixotropic character allowing for uniform, reproducible, and easily controlled gel structures. The weak bonds between aerosil particles leads to gels with soft elasticity, internal dynamics, and coupling to the host material or fluid. Thus, colloid dynamics, glasslike behavior, and rigidity can all be probed systematically as a function of gel density.

A particular compelling interest in such gels stems from their use in imposing quenched random disorder on liquid crystal (LC) phases [2]. In such LC+aerosil systems, the physics appears to be well described by a random-field approach [3,4]. It has also been shown that the dynamics of the host organic fluid and the aerosil gel are coupled [5]. A recent rheology study as a function of temperature and silica density of LC+aerosil samples found evidence of a rigidity transition in aerosil gels near 0.1 g cm^{-3} silica [6]. In fact, theoretical efforts have predicted the presence of long-range interactions among colloids mediated by the host fluid [7,8] and experimental studies have been made of the elasticity of the composite [9–11]. However, all previous studies cited have focused on the macroscopic behavior of the colloid; direct studies of the nature of the silica gel dynamics are lacking. Knowledge of the structure and dynamics of the aerosil particles themselves would greatly aid in the interpretation of their role in imposing disorder on such colloidal systems. In addition, direct studies would illuminate the process of rigidity as a function of densification in fractal-like gels.

Dynamic light scattering (DLS), a widely used and well-known speckle technique [12] in the visible region of the spectrum, has been used to study the dynamics of orientational order fluctuations of LCs in LC+aerosil dispersions [13]. However, LC+aerosil samples can become quite turbid (multiple-scattering regime) with a small increase in sil concentration, necessitating very thin samples that compromise the dispersion homogeneity. In addition, DLS typically cannot probe the fluctuation dynamics on a length scale smaller than about 200 nm.

The x-ray analog to DLS, x-ray intensity fluctuation spectroscopy (XIFS; also called x-ray photon correlation spectroscopy), enables access to higher momentum transfer q by means of the shorter photon wavelengths, and does not suffer from the multiple-scattering limitations of DLS [14]. X-ray speckle methods such as XIFS have only recently become feasible with the advent of x-ray undulator sources at third-generation synchrotron facilities [15–18]. As for DLS, spatially and temporally coherent illumination of the sample is required. Although lasers do not yet exist in the x-ray region of the spectrum, an intense, highly coherent x-ray beam can nonetheless be obtained by isolating the coherent from the incoherent portion of an undulator beam using apertures and monochromatization.

Using the high flux of coherent x-ray photons from an undulator source, XIFS can directly probe the dynamics of disordered systems down to atomic length scales and on time scales down to milliseconds [19]. The use of fast charge-coupled device (CCD) area detectors in XIFS enables extraction of both spatial and temporal information in one single

*Electronic address: gsiannac@wpi.edu

experiment by multispeckle methods. This approach offers several advantages for the study of nonergodic and slow processes: the sample does not need rotation, improving the statistics of the data [20], and the measurement time can be decreased to the longest relaxation present in the sample [21,22]. XIFS has been particularly valuable for the study of slow dynamic phenomena in soft condensed matter.

Here, we present an XIFS study of the structure and dynamics of the aerosil gel dispersed in the liquid crystal octylcyanobiphenyl (8CB) as a function of silica density. The fact that the aerosil forms a fractal gel structure, which holds its shape even in the isotropic phase of the LC indicating its robustness, is crucial because the analysis and interpretation of the optical and calorimetric data [4,23] is based on the hypothesis that the resulting aerosil gel structure does not age. However, a previous XIFS study of one LC+aerosil sample did reveal very slow dynamics that appeared coupled to the particular liquid crystal phase [5]. The focus of this work is to explore the silica density dependence of the gel dynamics in a LC+sil colloid in order to make direct connection with these previous studies.

The experiments were performed at a fixed temperature deep in the smectic-*A* (Sm*A*) phase of 8CB. Since the Sm*A* structure of the host is well established, we assume that the liquid crystal nature of the fluid does not play an important role. The viscous nature of the medium and the elastic coupling to the gel should be the only significant features. The aerosil gels studied here are found to have generally stable fractal structures with some indications of aging for one sample. Dynamics of the gel are clearly observed with extremely long characteristic relaxation times that are aerosil density dependent. It is expected that the characteristic relaxation times of the gel dynamics should monotonically increase with increasing silica density due to the increasing connections among the aerosil gel strands. The ultimate limit of a semi-infinite relaxation time (near-zero dynamics) would be expected to occur at complete solidification, at silica density approaching that of pure silica (2.2 g cm^{-3}). However, the observed density dependence of the aerosil gel dynamics is more complex. The gel dynamics do slow down with increasing aerosil density immediately above the percolation threshold of $\approx$0.015 g cm^{-3}, but then the system enters a glassy region for densities $\gtrsim$0.08 g cm^{-3} with the appearance of two relaxation times. The situation changes dramatically for the highest-density sample, 0.20 g cm^{-3}, which exhibits a different structure and faster dynamic behavior than the lower-density samples. It is not clear whether these faster dynamics represent a distinct underlying mode, revealed when the more dominant relaxation mode was arrested, or the speeding up of the same dynamic mode. There does appear to be a narrow region of aerosil density, between the percolation threshold and $\approx$0.10 g cm^{-3}, where a very rigid glasslike phase of the nanocolloidal gel exists.

This paper reviews the details of the experimental procedures and samples in Sec. II and presents a description of the results in Sec. III. A discussion of these results is presented in Sec. IV. The paper concludes with a brief discussion of future experimental and theoretical directions.

II. EXPERIMENTAL PROCEDURES

A. XIFS experiment

The XIFS experiments were conducted in the transmission geometry using the XOR 2-ID-B undulator beamline at the Advanced Photon Source at Argonne National Laboratory [24]. The beamline focusing mirrors and spherical grating monochromator delivered the undulator beam to the experiment with a footprint size of a few hundreds of micrometers. The typical transverse coherence width of the beam during this experiment was $\sim$25 μm using monochromator entrance and exit slit openings of 200 and 50 μm, respectively. The coherence width could be increased by further closing the slits, but at considerable expense of photon flux.

The coherent part of the x-ray beam was selected by a 10 μm pinhole. A germanium guard edge located about 15 mm downstream of the pinhole blocked parasitic scattering from the pinhole. Gel samples were aligned to the coherent x-ray beam on a motorized two-axis stage, approximately 3 mm after the guard edge, mounted on the inner rotational axis (1θ arm) of a two-circle goniometer. The total distance from the pinhole to the sample was less than 2 cm to minimize air absorption and scattering of the x-ray beam. The typical spectral coherent flux incident on the sample was 3×10^7 photons/s per 0.1% BW (relative bandwidth).

The sample holder consisted of two copper plates, each with a small hole over which was glued a 200-nm-thick, 0.7×0.7 mm^2 silicon nitride x-ray window [25]. A thin layer of gel sample was spread over one of the windows; then the plates supporting the windows were clamped together with screws. The windows were aligned with one another using an optical microscope to obtain the maximum possible area exposed to the beam. The assembled holder was clamped in a copper block; its temperature was monitored with a thermocouple. The experiments were carried out at room temperature (300.75$\pm$0.5 K).

The x-ray speckle patterns produced by the sample were detected by a CCD camera mounted on the goniometer 2θ arm at a distance of $\approx$95.0 cm from its center and at angle 2θ=0.82° from the direct beam. The 16-bit CCD camera, made by Princeton Instruments, was modified to extend its vacuum envelope and to replace its quartz optical window with a silicon nitride x-ray window. The camera used a SITe CCD chip, 1024×1024 pixels, 24×24 μm^2 in size and cooled to −120 °C. This configuration covered momentum transfers (q) ranging from 0.02 to 0.2 nm^{-1}. Figure 1 shows the scattering geometry and CCD location with respect to the direct beam. However, for the autocorrelation analysis, only full arcs through the CCD image were taken, limiting the q range to 0.03–0.15 nm^{-1} (corresponding to length scales from 42 to 209 nm).

In order to maximize the speckle contrast from the aerosil gel, the x-ray energy was chosen to be 1.830 keV, just below the Si *K* absorption edge [26]. This ensured that the patterns obtained were primarily due to scattering from the aerosil. Experimentally, sample regions with $\sim$25% absorption gave the best speckle contrast. Time series of $\sim$30 s speckle exposures with $\sim$6.4 s between exposures were recorded over

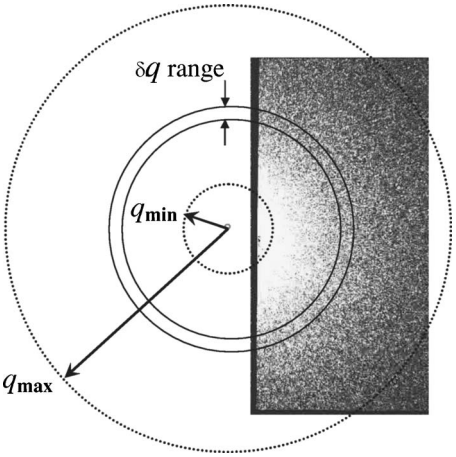

FIG. 1. Schematic of the full CCD image relative to the scattering geometry. Image shown is that for the 0.08 sample at room temperature. The δq range (exaggerated here) is about a mean wave vector $\bar{q}$ over which the autocorrelation "boxes" are averaged.

a 4–9 h run for each sample (400–900 exposures). No apparent radiation damage to the samples was observed during the time series. The absolute time, storage ring current, beamline settings, guard edge position, sample temperature, and sample position were stored with each CCD exposure when it was recorded. Several times during the experiment the guard edge drifted on the order of 1 μm, possibly due to thermal variations of the apparatus. This was mitigated by periodically adjusting the guard edge position.

The data reduction and calculation of the time autocorrelation function at each wave vector position q,

$$g^{(2)}(q,\Delta t) = \frac{\langle I(t)\rangle_q \langle I(t+\Delta t)\rangle_q}{[\langle I(q)\rangle_q]^2}, \tag{1}$$

followed the scheme suggested by Lumma *et al.* [21] and included corrections for the storage ring current, the total speckle intensity, and the CCD dark level. Corrections were made with respect to the dark level and damaged pixels of the CCD. Also, all the pixels of each subsequent exposure in the series were scaled to the ring current and the total intensity of the first exposure on a pixel by pixel basis. This type of scaling reduced the effects of beam instabilities and intensity changes at the sample.

The speckle data were initially analyzed to find the proper size of the autocorrelation box for subsequent analysis. The size of the autocorrelation box was adjusted to match closely with the average speckle size, which was calculated from the average spatial autocorrelation function

$$g^{(2)}(\Delta q) = \frac{\langle I(q) I(q+\Delta q)\rangle_q}{[\langle I(q)\rangle_q]^2} \tag{2}$$

of several speckle patterns. The average speckle size was found to have a radius of ~ 3 pixels and this was used as the box size for the analysis presented in this paper.

The time intensity autocorrelation function was then calculated for each box (from the same position in the speckle pattern) in the time series. A second reduction was then done by calculating the average time autocorrelation function for all boxes that lie in the same $q \pm \Delta q$ range. This resulted in the final $g^{(2)}(q,\Delta t)$ for a specific q. To improve the statistical accuracy, the multi-τ method of Schätzel with symmetric normalization was adopted [27–29].

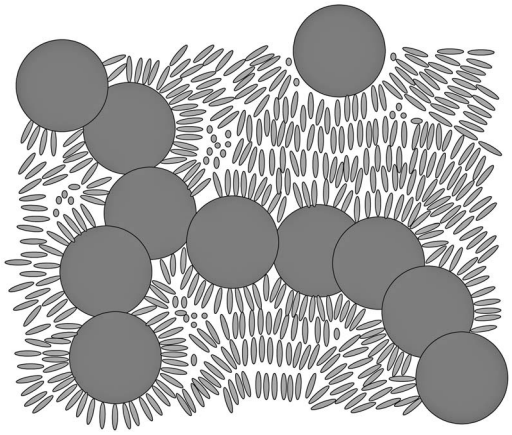

FIG. 2. Cartoon of a LC+aerosil gel approximately 47 nm across (based on an individual aerosil sphere being 7 nm in diameter), which is near the lower end of the length scales probed in this work, illustrating the relative sizes of the silica sphere and 8CB molecule. The gel forms long, necklacelike, chains that interconnect randomly and percolate to form a gel at densities $\gtrsim 0.02$. The polar LC molecules have a more or less homeotropic alignment at the silica surface.

B. LC+aerosil samples

The 8CB liquid crystal used in this work is a well-studied prototypical rodlike molecule, with a rigid biphenyl core at one end attached to an aliphatic tail and at the other to a polar cyano group. Its molecular weight is $M_w = 291.44$ g mol^{-1}. The pure material undergoes a weak first-order isotropic-to-nematic transition at $T^o_{IN} = 313.98$ K, a continuous nematic to smectic-A transition at $T^o_{NA} = 306.97$ K, and crystallizes below 290 K [2,30]. The aerosil consists of SiO_2 (silica) spheres about 7 nm in diameter, coated with (-OH) hydroxyl groups. The coating enables the spheres to hydrogen bond and form a thixotropic [31] fractal gel in an organic solvent such as 8CB.

A cartoon of the aerosil gel and LC molecules, drawn approximately to scale, is shown in Fig. 2. The gel can be thought of as randomly crossing long silica chains with very high pore volume fraction and no preferred orientation, as was shown by light scattering [23] and small-angle x-ray scattering (SAXS) studies [2]. However, these SAXS studies showed that the basic aerosil unit consists of a few of these spheres fused together during the manufacturing process [2]. The specific surface area of the type-300 aerosil is $a \approx 300$ m^2 g^{-1} determined by a Brunauer-Emmett-Teller adsorption isotherm as specified by the manufacturer. The gelation threshold for the aerosil used in this experiment occurs approximately at a silica density of $\rho \approx 0.015$ g cm^{-3}. Because of the surface hydroxyl groups, the polar 8CB molecules should anchor homeotropically at the silica surface. However, due to the small radius of curvature and expected

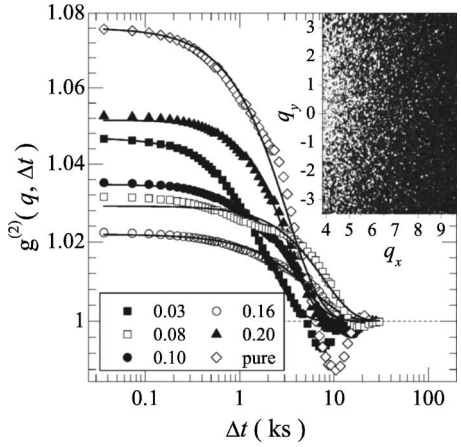

FIG. 3. Time autocorrelation curves for different aerosil densities at $\bar{q}=0.051$ nm^{-1} ($\bar{d}\sim 125$ nm). The solid lines represent typical fits using Eq. (3) with β free. The inset shows an enlarged section of the image for the 0.08 sample shown in Fig. 1 where q_x and q_y are in units of 10^{-2} nm^{-1} (250×300 pixels) illustrating typical speckles.

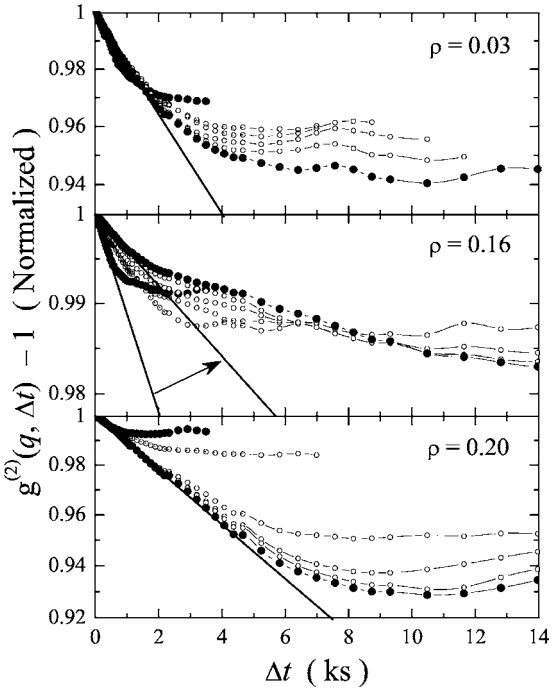

FIG. 4. Buildup of the time autocorrelation function whose amplitude was normalized to 1 with increasing sample time for three 8CB+aerosil dispersions. The solid circles denote the normalized $g^{(2)}-1$ for 100 images ($\sim$1 h) and for 800 images ($\sim$8 h). Open circles present a few autocorrelation functions at intermediate times illustrating the buildup of the baseline B. Note that the 0.16 sample does not exhibit a common initial slope as do all the other samples studied.

undulations of the silica surface, the actual surface orientation is most likely tilted.

The silica density dependence of the aerosil gel dynamics was studied in six dispersion samples of LC+aerosil ranging from 0.03 to 0.20 g cm^{-3} (grams of silica per cm^3 of total volume; the units are dropped hereafter). In addition, a pure aerosil gel sample of unknown density was also studied. Each dispersion sample was dissolved in very-high-purity acetone and sonicated for more than 1 h to produce a microscopically dispersed mixture. The acetone was then slowly evaporated over several hours, allowing gelation. The samples were subsequently dried under vacuum for more than 2 h at elevated temperature. This preparation method has been shown to produce uniform and reproducible dispersions [2].

A thin layer of each LC+aerosil sample in several thicknesses was spread onto silicon nitride x-ray windows on copper holders and sealed as described above. The pure aerosil sample was prepared by sprinkling a thin layer of aerosil onto the silicon nitride window. The pure aerosil was held in place by electrostatic forces. All experiments were carried out essentially isothermally in the smectic-A phase of 8CB, so the coupling between the LC host and aerosil gel would be the same for all samples. This should isolate the density dependence of the aerosil gel dynamics.

III. RESULTS

Fluctuating speckles were clearly observed in all time series. Figure 3 shows $g^{(2)}(q,\Delta t)$ at $q=5.1\times 10^{-2}$ nm^{-1} for each sampled studied. The time autocorrelations generally show low contrast (less than 10%) and long relaxation time (on the order of several times 10^3 s). Although there do appear indications of two relaxation times, especially for the 0.080 sample decay, the low contrast makes differentiating them difficult. As a result, a single effective relaxation time representing the average of the two relaxations was assumed in the analysis. Note that, in Fig. 3, $g^{(2)}(q,\Delta t)$ dips below 1, an indication of possible heterodyning between the scattered and the unscattered incident beam. The data for $\Delta t > 10^4$ s were thus considered to be unusable and were not included in the fitting analysis.

Because of the very long relaxation times, the effect of the finite experiment time on the shape of the autocorrelation can be profound. This distortion was characterized by analyzing the initial decay of the time autocorrelation function $g^{(2)}(q,\Delta t)-1$ that has its amplitude normalized to 1 for each experiment duration time (see Fig. 4). This analysis effectively shows the buildup of the autocorrelation baseline with time. The dependence of the relaxation time on the experiment duration is determined from a first-cumulant analysis or simple logarithmic slope of the initial decay. This estimate of the relaxation time, scaled to that found at 3.6 ks (1 h), is shown as a function of the experiment duration for all samples in the upper panel of Fig. 6 below. The initial decay times for the densities 0.03, 0.08, and 0.20 show some variations at small experiment times but tend to saturate after approximately 14.4 ks (4 h). However, the 0.16 and pure aerosil samples exhibit monotonically increasing relaxation times, suggesting that the autocorrelation function for these densities was not sampled even after 28.8 ks (8 h). These samples display speckles similar to those for the low- and high-density samples, but they are much slower, with relaxation times beyond the longest experimental time scales.

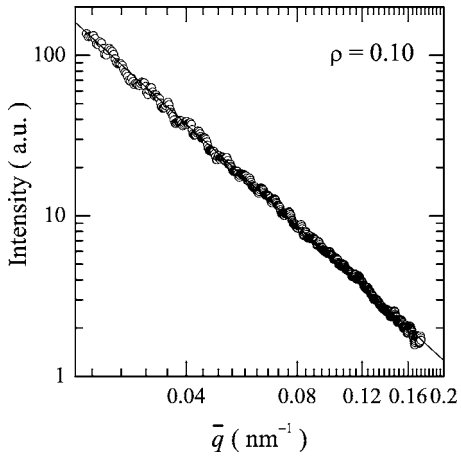

FIG. 5. Typical q dependence of the scattered x-ray intensity for the 8CB+sil samples. Shown is a log-log plot of the data for the 0.10 sample, averaged over 50 images at approximately 7000 s into the experiment. Solid line is a simple power-law fit yielding a dimensionality of d_f=2.107 for this sample.

Possible restructuring or aging of the gel structure for all samples was studied by tracking the time evolution of intensity as a function of wave vector, $I(q)$. Although the q range accessed by this experiment covered only one decade (using the entire q range accessible due to the limited CCD acceptance), the structure of the scatterers was well characterized for all images by a power law $I(q) \sim q^{-d_f}$, where d_f is the dimensionality (see Fig. 5). The lower panel of Fig. 6 shows the time evolution of the dimensionality of the aerosil gel structure. The average dimensionality for all samples is $d_f \approx 2.15$, which is consistent with an earlier SAXS study of the same dispersions [2]. Although the 0.03 and 0.08 samples show a very slow decrease in d_f with time, all higher-density samples and the pure aerosil sample d_f is essentially constant, indicating no significant restructuring.

The behavior of the 0.10 sample is unique. For the first 5 h of the experiment there appeared to be no significant changes in the dimensionality and a monotonically increasing effective relaxation time for the 0.10 sample similar to the results for the 0.16 and pure aerosil samples. But, in the last two hours, 0.10 exhibited a sharp decrease in the initial decay time (faster dynamics) and a correlated "bump" in the dimensionality (see Fig. 6). The origin of this behavior is unclear, but one possible interpretation is an avalanche of "stuck" states (internal frustrations) which, once freed, reveal faster gel dynamics [32].

In order to efficiently characterize the q dependence of the autocorrelation function for all samples over the whole lag time and for the entire experiment duration, a simple "stretched" exponential form is used:

$$g^{(2)}(q,t) = \Gamma_c \exp\left[-\left(\frac{t}{\tau}\right)^{\beta}\right] + B, \tag{3}$$

where the exponent β characterizes the nonexponential nature of the decay, τ is the characteristic (effective) decay time, Γ_c is the fluctuation contrast (strength), and B is the baseline value. The fit quality is reasonably good for most of

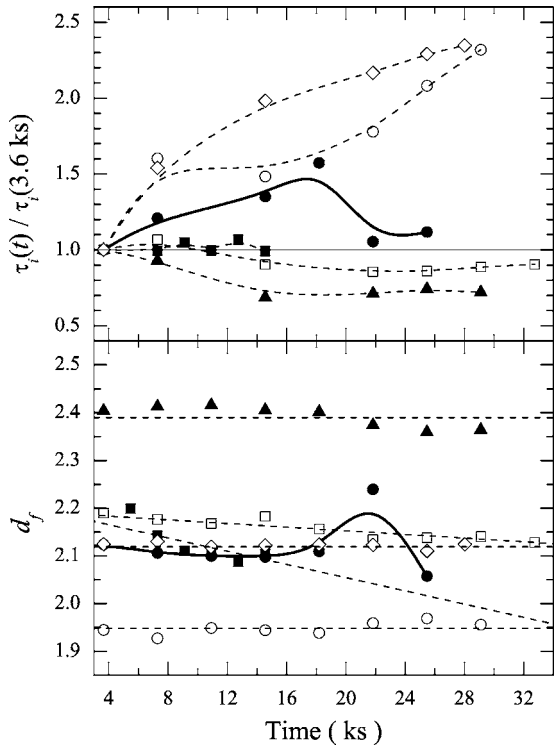

FIG. 6. Time evolution of the initial decay time τ_i, scaled by that found after 3600 s (upper panel) and the dimensionality d_f (lower panel) for the various gel samples. Symbols are defined by the inset in Fig. 3. The error in each quantity is on the order of the symbol size.

the samples except for the 0.08 sample, which exhibits two distinct relaxation processes (see Fig. 3) which interfere with a single-exponential relaxation description. The q dependence of the exponent β is plotted in Fig. 7. In general, the exponent β is near 1 for small q and increases with increasing q for samples with $\rho < 0.2$. This suggests faster than exponential relaxations for small length scales ($\lesssim$100 nm) and normal exponential relaxations for larger length scales. The exception is the 0.20 sample where β is larger than 1 for small q and approaches 1 with increasing q (decreasing length scale). This suggests that, while the 0.20 sample has nearly as fast dynamics as that for the 0.03 sample, the origin of these dynamics must be different. The characteristic decay times τ, obtained by fitting Eq. (3) to $g^{(2)}(q,t)$ with floating or fixed β, are similar to each other and show a dramatic dependence on the silica density, ranging from $\sim$1600 s at the lower density to above 7000 s in the glassy region.

The wave-vector dependence of the single characteristic decay time τ of $g^{(2)}(q,\Delta t)$ is shown in Fig. 8. Given the scatter and limited range, the log-log plot yields reasonably linear behavior consistent with a power-law dependence of the form $\tau \approx q^x$ for all samples studied. The upper panel shows the $\tau(q)$ behavior for the 0.08, 0.10, and 0.16 samples that are essentially constant (x=0) except for the 0.10 sample showing an x=0.23±0.05. The lower panel depicts the behavior for the 0.03, 0.20, and pure aerosil samples giving $x(0.03) = -0.30 \pm 0.08$, $x(0.20) = -0.50 \pm 0.05$, and x(aerosil) $= -0.71 \pm 0.06$. As with the relaxation time and fluctuation

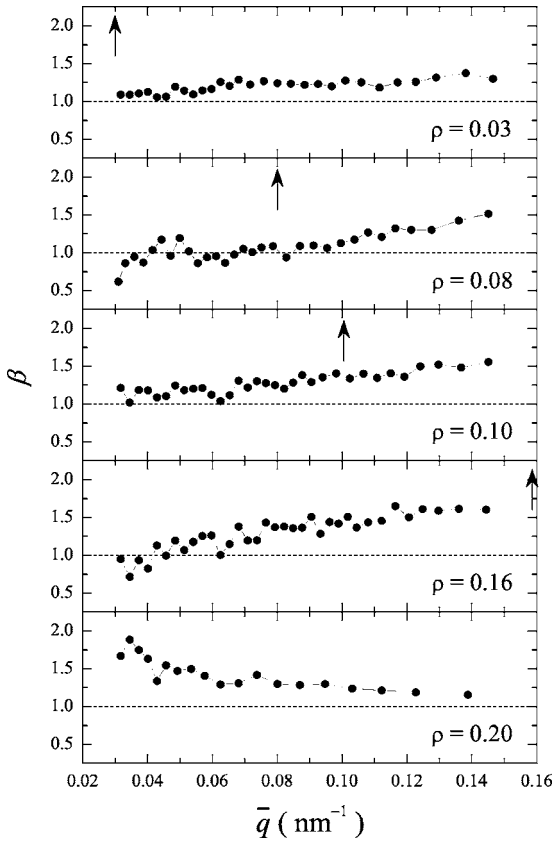

FIG. 7. The exponent β as a function of wave vector for the 8CB+aerosil samples extracted from fits using Eq. (3) to describe the two-point time autocorrelation decay $g^{(2)}(q,t)$. The pure aerosil sample resulted in a constant $\beta \simeq 1.4$ over the entire q range studied. The horizontal dashed line at $\beta=1$ in each panel indicates a pure exponential relaxation. The arrows indicate the wave vector q_m for each sample associated with the mean void size l_0 except for the 0.20 sample, which is off scale at $q_m=2\pi/l_0 \approx 0.21$ nm^{-1}.

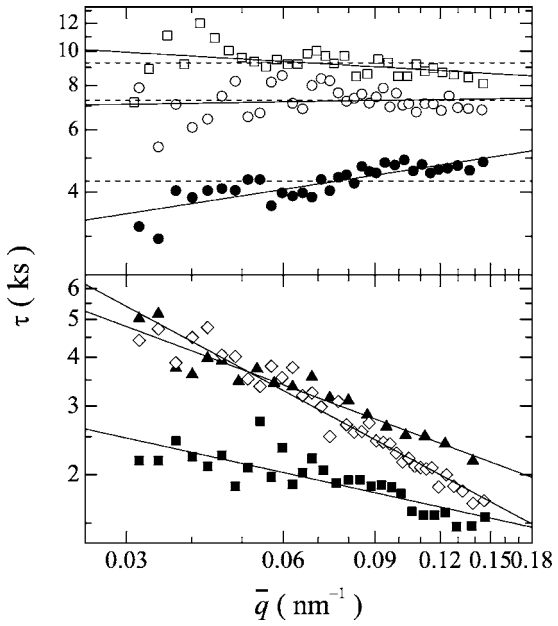

FIG. 8. Log-log plot of the single characteristic relaxation time τ_1 versus wave vector q. Symbols follow those in Fig. 3. Upper panel shows the dependence for 0.08, 0.10, and 0.16 samples with the horizontal dashed line indicating the q averaged value. Lower panel shows the 0.03, 0.20, and pure aerosil samples. The slopes of the solid lines in both panels indicate the exponent of a power-law relationship between τ_1 and q.

contrast, the $\tau(q)$ behavior in the aerosil density region about 0.10 differs from that below and above this density of the gel.

IV. DISCUSSION AND CONCLUSIONS

We studied the structure and dynamics of the aerosil gel in a liquid crystal host by XIFS at a fixed temperature over a spatial range of 42–209 nm and a time range of 37–28 800 s for silica densities from 0.03 to 0.20 g cm^{-3}. The gel structure is fractal with a dimension near 2.15 for most samples indicating a reaction-limited aggregation process [33]. However, the fractal dimension decreases with time for the 0.03 sample and approaches $d_f \simeq 2$ at a rate that decreases to zero for densities above 0.10. This suggests that the low-density gel ($\lesssim$0.10) restructures itself by expansion of the gel rather than compaction as might be expected in such tenuous "solids." The structure is completely stable for high-density gels ($>$0.10).

All gel samples studied exhibit dynamics of the silica even when the gel structure is static. A summary of the dynamics found in this study as a function of silica density is given in Fig. 9. The relaxation time τ increases dramatically with increasing silica density beginning at $\sim$1600 s for the 0.03 sample. The values found for τ for the 0.10 and 0.16 sample are lower bounds given the evolution of τ with time (see Fig. 4). Remarkably, the dynamics of the 0.20 sample recover to those observed in the 0.03 sample. See the middle panel of Fig. 9. This recovery is also seen in the evolution of the fluctuation contrast (strength) Γ_c for densities below and above 0.10. However, the character of these dynamics is different: the q dependence of the exponential relaxation form becomes progressively distorted with increasing density from 0.03 to 0.16 as quantified by the stretching exponent β. For the 0.20 sample, the behavior is reversed, with the relaxations becoming progressively purely exponential with increasing wave vector. Whether pure or modified exponential relaxation, the values for τ extracted from the analysis are stable.

The power-law dependence $\tau \approx q^x$ for the LC+sil and pure aerosil gels (though limited) as well as the exponent $\beta > 1$ are consistent with those seen in other colloidal gels [34–36]. However, the specific behavior of these aerosil gels appears to be more complex. It is expected that $x=-1$ for ballistic motion of a relaxation of local stress within the gel while $x=-2$ would indicate a diffusive propagation of such a fluctuation [37]. For the samples studied here over the limited range of q, neither description appears appropriate, although the pure aerosil sample appears to have nearly $x=-1$. This might indicate that some coupling to the host fluid is playing a role in the dissipation of the gel dynamics. It has been suggested that the exponent β is related to the mesh size (l_m) of the gel, $\beta<1$ or $\beta>1$ for length scales less

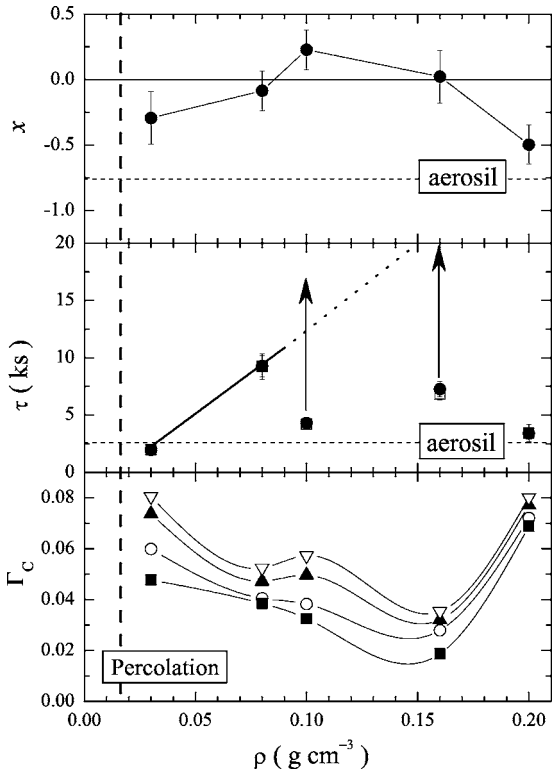

FIG. 9. Aerosil dynamics density dependence. Top panel: power-law exponent of the effective relaxation time wave-vector dependence. Middle panel: Effective relaxation time. Arrows indicate that τ has not saturated for the 0.10 and 0.16 samples; open squares are for a single-exponential ($\beta=1$) while solid circles are for a nonexponential (β free) analysis. Bottom panel: Fluctuation contrast $\Gamma_c(\rho)$ variation for different q (solid squares, 0.04; open circles, 0.06; solid triangles, 0.08; open diamonds, 0.10 nm^{-1}). All lines are guides to the eye and the dash-dotted lines represent the pure aerosil sample values. The vertical dashed lines indicates the expected percolation threshold.

than or greater than (respectively) the mesh size [36]. One possible measure of the mesh size for these gels is the mean void size l_0 [2,4]. However, the wave vector associated with $l_m=l_0$, $q_m=2\pi/l_0$, does not appear to correlate with any specific feature in $\beta(q)$ or $\tau(q)$. So, if some mesh size is involved with these gels, it was not probed by these experiments.

From the results obtained, a possible picture emerges of the aerosil gel structure and its dynamics which suggests a peculiar "transition" occurring near 0.10. In the low-density regime, the gel restructures itself continuously toward a lower-dimensional structure via events that propagate through the sample in a complex manner. This restructuring, though slow, achieves a steady-state equilibrium. In this view, the gel evolves continuously with no ground or final stable state. As the silica density increases, the restructuring slows until it enters a glassy regime before it is finally arrested. The dynamics in this regime are then a combination of the restructuring and intrinsic "vibrational" modes. Once the restructuring arrests in the high-density regime, only the vibrational mode remains. It is plausible to identify this intrinsic mode with vibrations of individual silica strands comprising the gel. The interconnections of the silica strands are random and should represent nearly fixed points. A vibration of a strand, initiated by some fluctuation of the host fluid or by some external noise, would propagate through the random gel. This would account for the coupling observed between the liquid crystal host and aerosil gel dynamics as a function of temperature [26].

These results clearly indicate that the physical characteristics of aerosil gels do not evolve smoothly with densification. As such, the effect of the aerosil gel on the host fluid should not evolve smoothly, and one should expect different liquid crystal behavior between the low- and high-silica-density LC+sil samples as has been found [2,4]. The results presented here imply a rich phase diagram for the aerosil gel with the observed behavior above and below 0.10 partitioning the aerosil gel into two regimes between the "gas-liquid"-like percolation threshold and true solidification (complete arrest of all silica gel dynamics) occurring at densities approaching that of pure silica. This transition near 0.10 may represent an initial rigidity transition at long length scales of the gel corresponding to the macroscopic rigidity observed by recent rheology experiments [6]. More experiments are needed in order to clarify the situation. Experiments with organic solvents of lower viscosity or conducted at higher temperature would shed light on the coupling to the host fluid. Also, faster speckle pattern acquisition would allow these dynamics and the initial part of the autocorrelation function below 30 s to be probed, as well as improve the statistics. These experimental improvements would open up studies of the evolution of restructuring processes, in particular discontinuities in densification.

ACKNOWLEDGMENTS

We wish to thank J. Arko and B. Tieman for their help with the experiments, C. W. Garland, R. L. Leheny, G. Phillies, and T. Bellini for many useful discussions, and C. Retsch for help with the IDL data-reduction software. This work was supported by the NSF-CAREER Grant No. DMR-0092786 and by the U.S. Department of Energy, Office of Science, Basic Energy Sciences, under Contract No. W-31-109-ENG-38.

[1] H. Sonntag and K. Strenge, *Coagulation Kinetics and Structure Formation* (Plenum Press, New York, 1987).
[2] G. S. Iannacchione, C. W. Garland, J. T. Mang, and T. P. Rieker, Phys. Rev. E **58**, 5966 (1998).
[3] R. L. Leheny, S. Park, R. J. Birgeneau, J. L. Gallani, C. W. Garland, and G. S. Iannacchione, Phys. Rev. E **67**, 011708 (2003).
[4] G. S. Iannacchione, S. Park, C. W. Garland, R. J. Birgeneau,

and R. L. Leheny, Phys. Rev. E **67**, 011709 (2003).
[5] C. Retsch, I. McNulty, and G. S. Iannacchione, Phys. Rev. E **65**, 032701 (2002).
[6] R. Bandyopadhyay, D. Liang, R. H. Colby, J. L. Harden, and R. L. Leheny, Phys. Rev. Lett. **94**, 107801 (2005).
[7] R. W. Ruhwandl and E. M. Terentjev, Phys. Rev. E **56**, 5561 (1997).
[8] H. Stark, Phys. Rep. **351**, 387 (2001), and references therein.
[9] P. Poulin, V. Cabuil, and D. A. Weitz, Phys. Rev. Lett. **79**, 4862 (1997).
[10] S. P. Meeker, W. C. K. Poon, J. Crain, and E. M. Terentjev, Phys. Rev. E **61**, R6083 (2000).
[11] I. I. Smalyukh, O. D. Lavrentovich, A. N. Kuzmin, A. V. Kachynski, and P. N. Prasad, Phys. Rev. Lett. **95**, 157801 (2005).
[12] P. N. Pusey, P. N. Segre, O. P. Behrend, S. P. Meeker, and W. C. K. Poon, Physica A **235**, 1 (1997).
[13] M. Bellour, A. Knaebel, J. L. Harden, F. Lequeux, and J. P. Munch, Phys. Rev. E **67**, 031405 (2003).
[14] D. L. Abernathy, G. Grübel, S. Brauer, I. McNulty, G. B. Stephenson, S. G. J. Mochrie, A. R. Sandy, N. Mulders, and M. Sutton, J. Synchrotron Radiat. **5**, 37 (1998).
[15] M. Sutton, S. G. J. Mochrie, T. Greytak, S. E. Nagler, L. E. Berman, G. A. Held, and G. Stephenson, Nature (London) **352**, 608 (1991).
[16] Z. H. Cai, B. Lai, W. B. Yun, I. McNulty, K. G. Huang, and T. P. Russell, Phys. Rev. Lett. **73**, 82 (1994).
[17] S. B. Dierker, R. Pindak, R. M. Fleming, I. K. Robinson, and L. Berman, Phys. Rev. Lett. **75**, 449 (1995).
[18] S. G. J. Mochrie, A. M. Mayes, A. R. Sandy, M. Sutton, S. Brauer, G. B. Stephenson, D. L. Abernathy, and G. Grübel, Phys. Rev. Lett. **78**, 1275 (1997).
[19] T. Seydel, A. Madsen, M. Tolan, G. Grübel, and W. Press, Phys. Rev. B **63**, 073409 (2001).
[20] J. Z. Xue, D. J. Pine, S. T. Milner, X.-l. Wu, and P. M. Chaikin, Phys. Rev. A **46**, 6550 (1992).
[21] D. Lumma, L. B. Lurio, S. G. J. Mochrie, and M. Sutton, Rev. Sci. Instrum. **71**, 3274 (2000).
[22] L. Cipelletti, S. Manley, R. C. Ball, and D. A. Weitz, Phys. Rev. Lett. **84**, 2275 (2000).
[23] T. Bellini, M. Buscaglia, C. Chiccoli, F. Mantegazza, P. Pasini, and C. Zannoni, Phys. Rev. Lett. **85**, 1008 (2000).
[24] I. McNulty, A. M. Khouusary, Y. P. Feng, Y. Qian, J. Barraza, C. Benson, and D. Shu, Rev. Sci. Instrum. **67**, 3372 (1996).
[25] Fabrication Services and Technology Ltd., JBJ Buisness Park, Northampton, U.K.
[26] C. C. Retsch and I. McNulty, Phys. Rev. Lett. **87**, 077401 (2001).
[27] K. Schätzel, M. Drewel, and S. Stimak, J. Mod. Opt. **35**, 711 (1988).
[28] C. J. Oliver, J. Phys. A **12**, 591 (1979).
[29] L. Cipelletti and D. A. Weitz, Rev. Sci. Instrum. **70**, 3214 (1999).
[30] J. Thoen, H. Marynissen, and W. VanDael, Phys. Rev. A **26**, 2886 (1982).
[31] A property of certain gels to become fluid when mechanically disturbed (as by shaking or stirring) and then reset after a period of time.
[32] H. Bissig, S. Romer, L. Cipelletti, V. Trappe, and P. Schurtenberger, Phys. Chem. Commun. **6**, 21 (2003).
[33] D. Asnaghi, M. Carpineti, M. Giglio, and M. Sozzi, Phys. Rev. A **45**, 1018 (1992).
[34] R. Bandyopadhyay, D. Liang, H. Yardimci, D. A. Sessoms, M. A. Borthwick, S. G. J. Mochrie, J. L. Harden, and R. L. Leheny, Phys. Rev. Lett. **93**, 228302 (2004).
[35] L. Cipelletti, L. Ramos, S. Manley, D. A. Weitz, E. E. Pashkovski, and M. Johansson, Faraday Discuss. **123**, 237 (2002).
[36] E. D. Gado and W. Kob, e-print cond-mat/0510690.
[37] A. H. Krall and D. A. Weitz, Phys. Rev. Lett. **80**, 778 (1998).